DOI: Not yet available. When the final version is published, the copy of record will be available on IEEE Xplore.

URL: Not yet available. When the final version is published, the copy of record will be available on IEEE Xplore.

Yves Mollet, Mathieu Sarrazin, Herman van der Auweraer and Johan Gyselinck

Université Libre de Bruxelles
Avenue Franklin Roosevelt 50 (CP165/52)
B-1050 Brussels
Belgium

Siemens Industry Software N.V
Interleuvenlaan 68
3001 Leuven
Belgium

Phone: +32 (0) 2 650 26 61
Fax: +32 (0) 2 650 26 53
Email: yves.mollet@ulb.ac.be

Investigation of the Influence of Open-Phase Faults on Noise and Vibrations of Switched Reluctance Machines

Yves Mollet
BEAMS department
Université Libre de Bruxelles
Brussels, Belgium
ymollet@ulb.ac.be

Mathieu Sarrazin
Product Lifecycle Management
Siemens Industry Software N.V
Leuven, Belgium

Herman Van der Auweraer
Product Lifecycle Management
Siemens Industry Software N.V
Leuven, Belgium

Johan Gyselinck
BEAMS department
Université Libre de Bruxelles
Brussels, Belgium

***Abstract*—Switched reluctance machines (SRMs) benefit from simple and cheap design and inherent fault tolerance, but still suffer from torque ripple and noise, vibration and harshness (NVH) issues. This paper experimentally investigates the influence of an open-phase fault on a 15 kW 8/6 SRM in terms of NVH and torque ripple by comparing run-ups with and without fault. The use of speed-frequency plots allows for an easy distinction between speed orders and structural resonances. Results show that even speed orders are amplified and damped in the vibration and sound-pressure-wave measurements in faulty and healthy conditions respectively. At low speeds, the sixth speed order also appears in the torque, due to the non-activation of one phase. This order however tends to disappear at high speed, due to the filtering effect of the mechanical inertia of the test bench.**

***Index Terms*—switched-reluctance machine, noise & vibration, open-phase fault, transient condition, spectrogram**

I. Introduction

SRMs are special machines having concentrated coils on salient stator poles and a salient winding-free and permanent-magnet-free soft-iron rotor. Torque is produced by successively activating stator phases to attract step by step the nearest rotor poles. Each of the phase activations is called 'stroke'. SRMs, previously limited to very specific applications, have gained attention in the last decades, since the development of power converters allows for their use in various state-of-the-art drive configurations, such as in automotive and aerospace applications [1].

Thanks to their simple stator construction and the absence of magnets and winding in the rotor, SRMs are particularly cheap [1]–[4], robust [2]–[5] and suited for severe environments [5]–[7] and high-speed applications [7]. SRMs also offer a high torque density [3] and very suitable torque-speed characteristics for electrical vehicles (EVs). The absence of permanent magnets also avoids depleting the limited available reserves of rare-earth elements [7], [8].

Thanks to the negligible magnetic coupling between the phases, SRMs also benefit from an inherent electrical fault-tolerance [3], [5], [7], [18]; this capability can be improved using fault-tolerant designs, such as modular machine and converter, combined with fault detection and isolation techniques [9]. The use of a machine with a high number of poles and parallel paths fed by separate H-bridge converters can be envisaged, but at the expense of increased complexity and costs [10]. The control can also be modified to increase the conduction intervals of the adjacent phases to compensate for the torque loss and specific strategies have been developed to start the faulty machine at any rotor position [12].

However, SRMs have to cope with some important drawbacks. First, their control strategies are complex, due to the fringing effect and the usually high magnetic saturation level during operation [7], and need a hardware or software position measurement [4], [13]. Second, the need of magnetizing the machine through the phase currents makes SRMs less efficient than permanent-magnet synchronous machines (PMSMs) and higher currents are needed to produce similar torques [5] Third, SRMs suffer from torque ripple and NVH issues [1]–[5], [7], [8], [12], caused by the discontinuous current in the phases [5], and the excitation of structural modes of the machine [8]. These drawbacks keep these motors from being extensively used so far compared to conventional induction machines and permanent-magnet synchronous machines, especially in noise-sensitive applications, such as EVs and HEVs.

As a consequence, the future development of SRM drives will depend on advanced techniques to measure, predict and counter their NVH concerns. An analytical model to predict radial vibration in SRMs is developed in [2] and used to compute the ensuing acoustic noise in [3]. AMESim software and FEA are coupled in [6] to successively estimate the working point of the SRM, the magnetic forces and the resulting vibrations and acoustic noise. Experimental tests are performed in transient conditions in [1] on a 12/8 SRM, and in [14] on a 12/8 and a 8/6 SRM, as well as on two PMSMs, in which further investigation of sound quality aspects and propositions to limit NVH issues are presented. In both references results are presented using speed-frequency plots (or spectrograms), so that frequency content related to speed can be easily distinguished from independent frequency content, such as external noise or resonance frequencies.

A larger air gap may be envisaged to reduce the radial

forces, but at the expense of a lower torque density. The torque ripple may also be reduced by skewing the rotor, but this is ineffective in big machines, due to production of torsional vibrations and associated noise [12]. As an alternative the control of the machine may be improved, e.g. by using torque-sharing functions, or an advanced converter topology [12].

The present paper focuses on open-phase faults, which can result from a manufacturing defect or the burnout of a weak point of the winding [10]. The action of a fuse in case of over-current or short-circuit also leads to an open-phase fault. An open-switch fault in the power converter also leads to a similar behaviour [18]. The influence of such a fault on noise and vibrations at various working points is investigated here. The frequency content of phase current, radial vibration, acoustic noise, and torque corresponding to speed ramps with and without fault are displayed as spectrograms, since they allow for a global visualization of frequency content at various working points, considering the advantages presented above.

Section II describes the main characteristics of the investigated machine and the main origins of vibrations. The test bench and its measurement set-up, as well as the implementation of the control are presented in Section III, while results are shown and discussed in Section IV.

II. Typical Waveforms and NVH Aspects of the Investigated SRM

A. Main Characteristics and Typical Waveforms

The rated and peak power, peak torque and peak current of the investigated 8/6 SRM are 15 kW, 30 kW, 200 Nm and 200 A respectively, while its maximum speed is 10 krpm.

In the frame of this work, average-torque control (ATC, activating one phase at a time) is used to drive the SRM. At low speed the desired torque is produced by chopping each phase current by means of a dedicated asymmetrical H-bridge converter, comprising two insulated-gate bipolar transistors (IGBTs) and two free-wheeling diodes, as shown in Fig. 1. In this paper soft chopping is used, i.e. one switch remains closed during the whole stroke, while the other one is switched to chop the current, its path being successively represented in Fig. 1a and b. At the end of the stroke both IGBTs are turned off and the magnetic energy stored in the phase is sent back to the DC-bus through both diodes according to Fig. 1c. A hysteresis control is here used to keep the current in a desired band ΔI^* around the reference I^*.

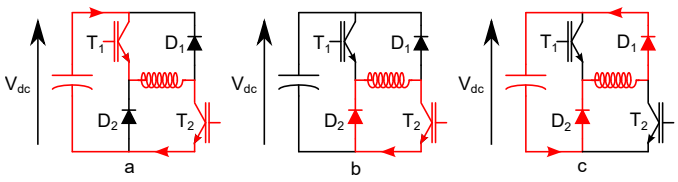

Fig. 1. Asymmetric H-bridge feeding one phase of the SRM: possible current paths. Depending on the states of both power switches T_1 and T_2, the applied voltage may be $+1$, 0 or -1 times the DC-bus voltage V_{dc} (cases a, b and c respectively).

Simulated flux-linkage, current and torque waveforms are presented in Fig. 2 for low, medium and high speeds. In the two first cases the current ripple related to chopping induces oscillations in the flux-linkage and torque waveforms, as shown in the blue and green curves in Fig. 2. A variation of the torque with rotor position at constant current can also be observed.

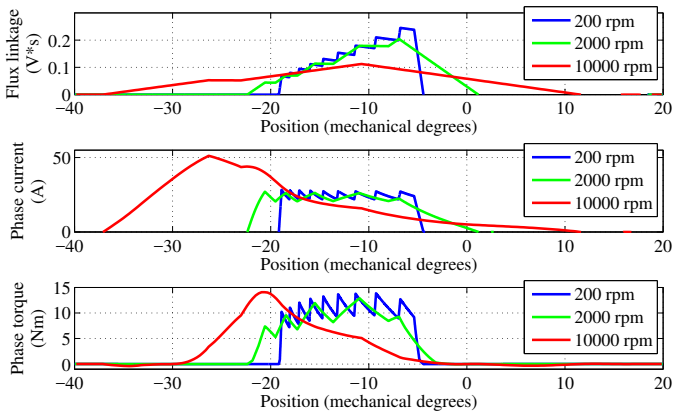

Fig. 2. Simulated flux linkage, current and torque waveforms corresponding to one phase of the investigated 8/6 SRM with 10 Nm load for different rotational speeds (in soft-chopping mode). The -30° and 0° rotor angles correspond to the unaligned and aligned positions respectively.

At medium speeds the pseudo-electromotive force (pseudo-EMF), i.e. the product of the angular speed and the derivative of flux linkage with respect to the rotor angle, tends to balance the supply voltage during the rising edges of the currents, whose slope decreases with speed. The consequence is a reduction of the amount of switching events during one stroke. In order to allow for a sufficient rise of the current, on the one hand, and avoid negative torque generation, on the other hand, the turn-on and turn-off angles θ_{on} and θ_{off} are also moved forward as the speed increases.

Beyond the base speed the pseudo-EMF overcompensates the supply voltage. The maximum average torque cannot be produced; only the rated power can be maintained and the current is then controlled (without any more chopping) by adjusting θ_{on} and θ_{off}.

B. NVH Aspects

Most of the vibrations in SRMs have their origin in pulsating magnetic forces between stator and rotor poles. Besides their tangential components, responsible for the production of torque, their radial components are the main cause of deformation of the stator yoke and its surrounding pieces and thus of the vibration of the machine [1]–[3], [15]. As a result, sound pressure waves (i.e. acoustic noise) are produced in the surrounding air. Vibrations are essentially produced during the commutations, their amplitudes increasing with the flux present at that time in the activated poles [2].

Two main types of frequency components can be distinguished. On the one hand, the successive activation of the phases is responsible for the apparition of fluctuating

components in the phase currents, air-gap forces and torque at multiples of the mechanical speed, i.e. speed orders. On the other hand, the hysteresis or PWM chopping of the phase currents at low speed also adds supplementary components at the switching frequency to torque and radial forces [1]. If a hysteresis controller is used to control the current or the torque, the switching frequency fluctuates in time and depends on chopping mode or hysteresis bandwidth, and to a minor extent on speed.

The pulsating forces described above may also excite the resonance modes of the stator and of other components of its environment such as, if present, the cooling jacket [1], [2], [14], [15]. Considering the stator as a cylindrical shell without constraints at both ends, different circumferential modes shapes with their corresponding order m and frequencies can be computed [15]. However, the presence of the poles, end caps and coils, and the motor mounting can change the stiffness of the system and thus affect the natural modes and associated frequencies [1], [15]. According to the working principle of the motor, the order m of the dominant circumferential mode corresponds to the ratio between the number of stator poles and phases [5]. In the case of the 8/6 SRM, having one pair of opposite stator poles per phase, each activation of a phase excites mainly the ovalization mode ($m = 2$). Furthermore, referring to the contribution of phase 1 to this mode shape, the action of phase 3 is opposite and phases 2 and 4, situated on nodes of the considered deflection shape act on an independent and 45-degree-sifted mode shape [17]. Therefore, the odd multiples of the fundamental frequency of the phases tend to excite the mode, while the even multiples correspond to in-phase actions of phases 1 and 3 and therefore tend to cancel the displacement.

III. Measurement Set-Up and Implementation of the Control

A. Measurement Set-Up

This paper investigates the influence of an open-phase fault on current, radial vibration, acoustic-noise and torque spectra of the SRM. This impact is evaluated experimentally comparing run-ups in healthy and faulty cases with each other (in no-load condition and when a 5 Nm load is applied). The test bench is composed of the investigated SRM, a 7.5 kW DC machine, used as a load and their converters. The electrical circuit of the bench is presented in Fig. 3. The microphone and accelerometer used for the present tests, as well as the current sensors, are encircled in yellow in Fig. 4. Due to its compact dimensions the SRM is normally cooled by water, while the DC machine is air-cooled by means of a dedicated fan. The cooling systems are, however, not activated during the tests to prevent additional frequency components to be superposed on the investigated vibrations and acoustic noise. This configuration is permitted by the short duration of the tests.

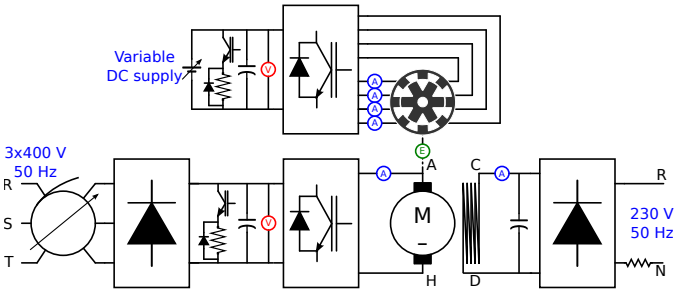

Fig. 3. Main electrical circuit of the SRM test bench. The SRM is controlled using its dedicated converter, while the DC machine is fed by an H-bridge converter.

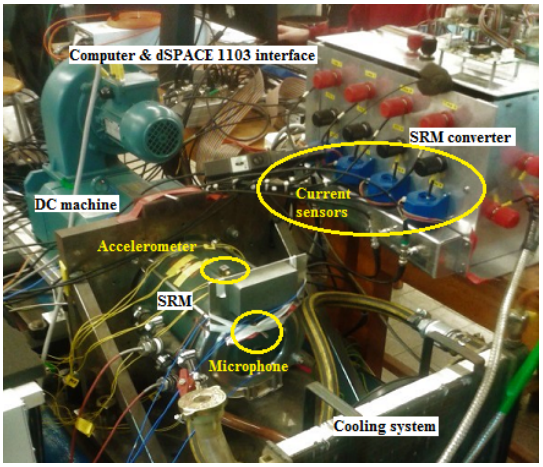

Fig. 4. Principal components of the experimental setup.

B. Structure and Implementation of the Control

The control of the SRM, as well as the one of the DC machine via classical cascaded PI controllers for speed and torque/current control are implemented in MATLAB/Simulink environment and uploaded on 1103 dSPACE fast-prototyping hardware, having a sampling rate of 10 kHz. The hysteresis needs however a higher sampling frequency (200 kHz) to avoid degraded performance [16] and is implemented on external STM32F4-Discovery-microcontroller cards.

The overview of the implementation of the ATC of the SRM on both hardware platforms is presented by the dashed rectangles in Fig. 5. A classical PI controller compares the speed with its reference and outputs the torque set-point. This value is used with the measured speed as input of three look-up tables (LUTs) computing I^*, θ_{on} and θ_{off}. The measured rotor position (in electrical degrees) θ_{elec} is then compared with θ_{on} and θ_{off} to output the phase-activation flags, which are sent together with the current references, a Boolean variable for hard- or soft-chopping selection and the hysteresis-bandwidth reference ΔI^* from dSPACE to the external microcontrollers, responsible for the current-hysteresis control.

Each phase current reference is directly compared to the output from the sensor, and the resulting error enters a hysteresis controller, which outputs a binary signal. If the phase is

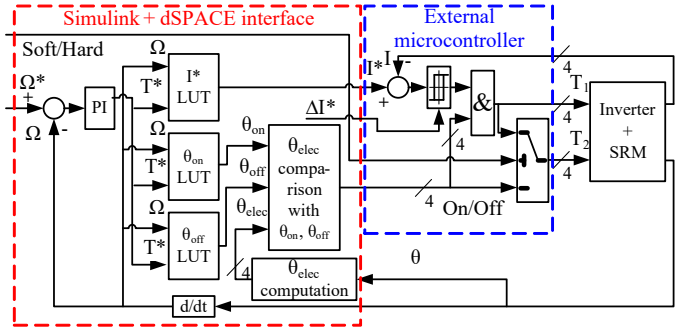

Fig. 5. SRM test-bench control structure. The T_1 and T_2 inputs of the 'Inverter + SRM' block refer to the gate signals of the upper and lower power switches in Fig. 1.

activated, its corresponding signal goes through the AND gate and is used to control the switches of its H-bridge. In hard-chopping mode the signal is duplicated so that both IGBTs (T_1 and T_2) operate together, while in soft-chopping mode the phase-activation flag is used to control one of the IGBTs (T_2 for example), which then remains closed during the whole stroke.

IV. Experimental Results

In order to excite a large range of frequencies and highlight the influence of speed on results [1], run-ups from 50 to 2000 rpm are performed in healthy and faulty cases with a rate of 25 rpm/s. The DC-bus voltage of the SRM converter and the hysteresis bandwidth are set to 300 V and 2.5 A respectively. During the tests, the SRM is speed-controlled while the torque is imposed by the DC machine.

The phase current, vibration and acoustic noise are first acquired in function of time. By applying a sliding (short-time) window to the signal, fast-Fourier transforms (FFTs) are performed to get the frequency content (RMS values) in function of time, as explained in [19]. Due to speed oscillations present in the original signal, these results are then sorted in increasing order and finally interpolated according to a regularly growing speed profile, to be finally plotted as spectrograms. The spectrum of the torque is estimated from the armature and excitation currents of the DC machine.

A. Healthy case

The spectrograms of phase current, radial vibration and acoustic noise, on the one hand, and of the torque on the other hand, corresponding to a run-up of the healthy SRM with 5 Nm load are presented in Fig. 6 and 7 respectively. The sampling frequency of the measurements used for the plots is 102.4 kHz. The frequency and speed resolutions of the spectrograms are 6.25 Hz and 1 rpm respectively.

The current plot of Fig. 6 is essentially composed of speed orders, forming oblique green to red lines going through the origin {0 kHz, 0 rpm}. Only multiples of the 6th order, corresponding to frequencies multiple of 100 Hz at 1000 rpm, are present in the current, since the current waveform is repeated each time a rotor pole is passing along the excited stator pole

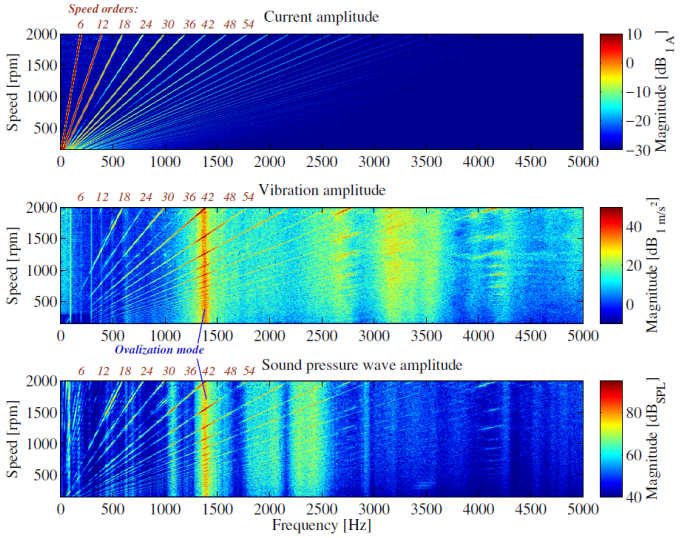

Fig. 6. Phase current, radial vibration and acoustic-noise frequency content (speed-ramp test, soft chopping, 5 Nm load, healthy case). The 0 dB references are 1 m/s^2, 1 A and 20 μPa respectively.

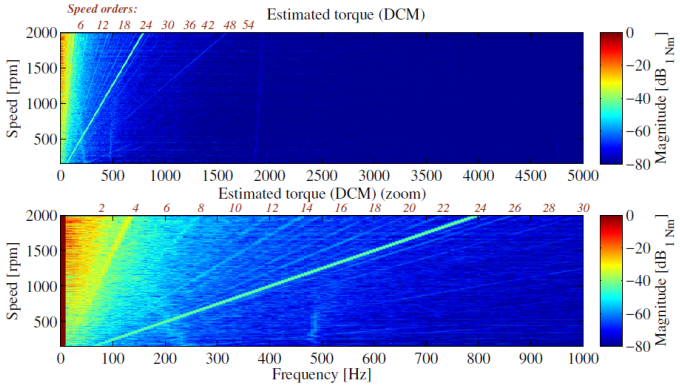

Fig. 7. Estimated torque frequency content (speed-ramp test, soft chopping, 5 Nm load, healthy case). The lower plot is an x-zoom of the upper one for frequencies up to 1 kHz. The 0 dB reference is 1 Nm.

(i.e. six times per revolution). The very low amplitude of the 24th order and of its multiples at low speed (corresponding to frequencies multiple of 400 Hz at 1000 rpm) can be explained by the fact that the current waveform is close to a square signal with a fundamental being six times the rotation frequency and with a 0.25 duty-cycle; using a simple Fourier-series analysis, it can be indeed proved that such a square signal does not have harmonics multiple of 4. The apparition of the 24th order and its multiples at high speeds can be explained by the change in the current waveform illustrated in Fig. 2.

Since the radial forces generated by the current act as a vibration source, the current content can also be found on the vibration plot. However, vertical bands (i.e. frequency content independent from speed) due to resonance of the SRM or of other components of the bench also appear. The most remarkable one is the high amplitude line near 1.4 kHz, which corresponds to the dominant ovalization mode of the machine [6]. As expected, in the neighbourhood of the resonance

frequency corresponding to ovalization mode, odd and even multiples of the 6th speed order are amplified and damped respectively [17].

The speed orders and the resonance at 1.4 kHz are also visible on the acoustic noise plot. However, some other components at constant frequency differ from the vibration plot, since they are probably produced by the resonance of accessory pieces of the SRM.

The amplitudes of the torque fluctuations presented on the top part of Fig. 7 are very low, except at low frequencies; a zoom of this region is presented in the bottom plot. It comprises a relatively continuous zone with high amplitudes growing with speed up to 100 Hz at 2000 rpm. Some speed fluctuations during the tests may contribute to the generation of these frequencies. Moreover, some misalignment between both machines of the bench may also produce torque fluctuations corresponding to the first and second speed orders. The second speed order may furthermore be also produced in the armature current of the 2-pole DC machine. The order 4, which can be distinguished in the bottom part of Fig. 7, may be considered as a harmonic of the fluctuations at twice the mechanical frequency. Finally, the orders 24 and 48, visible on both plots, result from the use of ATC control with a machine having 24 strokes per rotation.

B. Faulty case

The spectrograms corresponding to the run-up in the same conditions as presented above, but with an open-phase fault are presented in Fig. 8 and 9. While the current plot (of one of the remaining healthy phases) in Fig. 8 remains close to the one in Fig. 6, the even harmonics of current are much more visible in the vibration and acoustic-noise plots, due to the asymmetric character of the excitation. They are also amplified, when crossing the resonances (e.g. at 1.4 kHz), but generally less than the odd orders, probably since they still partially cancel each other. A global reduction of amplitudes above 3.5 kHz is also observed, whereas very-low-frequency components (below 200 Hz) are present in acoustic noise.

The torque spectrum presented in Fig. 9 differs from the one in Fig. 7 by the apparition of the 6th speed order, generated by the torque ripple resulting from the non-activation of one phase. This order however disappears at speeds higher than 1000 rpm, due to the filtering effect of the mechanical inertia. This corroborates the reduction of speed ripple at high speed observed in [11]. The amplitude of the order 24 seems, however, to remain constant. In that case the filtering effect of the inertia is compensated by the change in the torque waveforms, which moves away from a square wave (cf. Fig. 2); the ripple at the stroke frequency in the output torque grows as the speed increases, as shown in [12]. Below 500 rpm the 12th and 18th orders are also visible.

Besides the spectrograms, the spectra at 500 rpm are displayed for run-ups with and without open-phase fault at no-load and at load in Figure 10. This plot can be regarded as the two-dimensional representation of slices of waterfall diagrams at the investigated frequency. For visibility purposes,

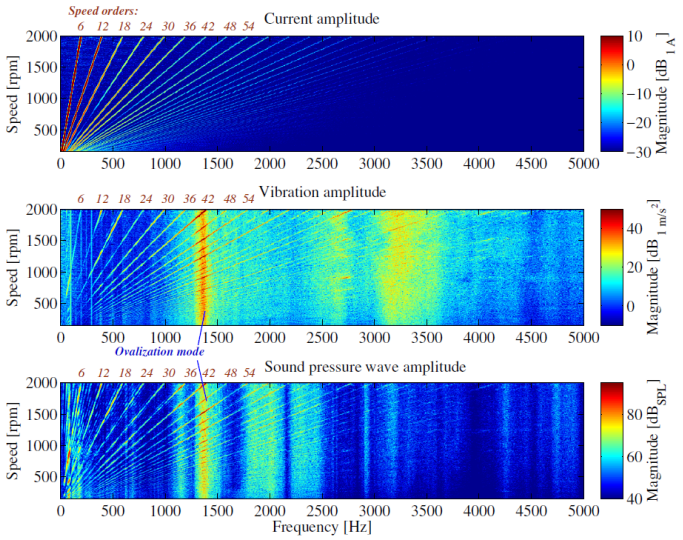

Fig. 8. Phase current, radial vibration and acoustic noise frequency content (speed-ramp test, soft chopping, 5 Nm load, one phase open). The 0 dB references are 1 m/s^2, 1 A and 20 μPa respectively.

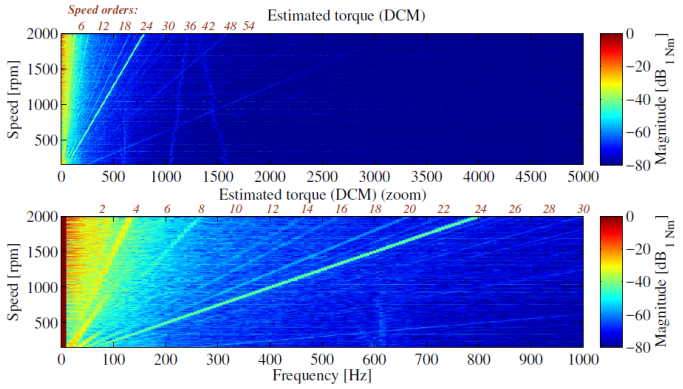

Fig. 9. Estimated torque frequency content (speed-ramp test, soft chopping, 5 Nm load, one phase open). The lower plot is an x-zoom of the upper one for frequencies up to 1 kHz. The 0 dB references are 1 Nm.

the frequency range is limited to the 0 - 1 kHz range, for which the amplitudes are the highest.

As expected, the orders with frequencies multiple of 200 Hz have smaller amplitudes than the others in the current plots. The application of the load generates an increase of vibration and acoustic noise amplitudes in the whole frequency range due to the increase of phase current amplitudes. In the vibration and acoustic-noise plots the additional peaks at load with open-phase fault with respect to the healthy case have to be related to the supplementary oblique lines in Fig. 8, i.e. to the even speed orders. However, no remarkable difference appear between the unloaded cases with and without fault. Regarding the torque, the additional peak at 50 Hz (6th speed order) appears on the faulty case besides the already present one at 200 Hz (24th order) in the healthy case.

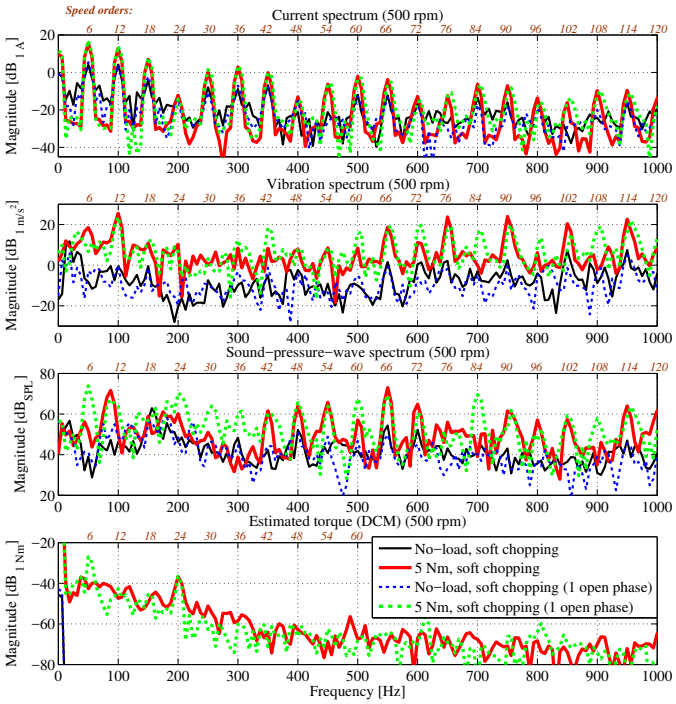

Fig. 10. Comparison of the FFTs of the phase current, radial vibration, acoustic noise and estimated torque at 500 rpm for no-load and 5 Nm load cases (soft chopping) with and without the presence of one open-phase fault.

CONCLUSION

The influence of open-phase faults on NVH aspects of a 15 kW 8/6 SRM has been experimentally investigated by comparing the frequency content of phase current, vibration, acoustic noise and torque during run-up tests. Results at load with and without the fault have been plotted as spectrograms together with an FFT comparing all test cases (including the no-load cases) at 500 rpm.

In case of an open-phase fault a slight global decrease of noise and vibration amplitudes is observed. Moreover, due to the asymmetrical excitation of the machine, even current orders are much more visible in the vibration and acoustic-noise plots and also interact with the structural resonances, but in a lesser extent than odd ones. The 6th speed order also appears in the torque estimation, but tends to be damped when the speed increases.

ACKNOWLEDGMENT

The authors would like to thank the Wallonia-Brussels Federation and the National Authority for Research of the Romanian Government for supporting this research via the cooperation project “Hardware-in-the-loop testing of variable reluctance machines for low-noise automotive applications”.

REFERENCES

[1] M. Sarrazin, S. Gillijns, K. Janssens, H. Van Der Auweraer and K. Verhaeghe, “Vibro-acoustic measurements and techniques for electric automotive applications,” INTER-NOISE and NOISE-CON Congress and Conference Proceedings, Institute of Noise Control Engineering, vol. 249 no. 2, pp. 5128-5137, 2014.

[2] C. Lin, B. Fahimi, “Prediction of radial vibration in switched reluctance machines,” IEEE Transactions on Energy Conversion, vol. 28, no. 4, pp. 1072-1081, 2013.

[3] C. Lin, S. Wang, B. Fahimi, “Efficient multiphysics modelling of vibration and acoustic noise in switched reluctance motor drives”, Proceedings of the 40th Annual Conference of the IEEE Industrial Electronics Society (IECON 2014), IEEE, Dallas, TX, USA, pp. 542-548 29 October 1 November 2014.

[4] P. Rafajdus, A. Peniak, D. Peter, P. Makys, and L. Szabó, “Optimization of switched reluctance motor design procedure for electrical vehicles,” in Optimization of Electrical and Electronic Equipment (OPTIM), 2014 International Conference on, pp. 397-404, 2014.

[5] Z. Yang, F. Shang, I.P. Brown, M. Krishnamurthy, “Comparative study of interior permanent magnet, induction, and switched reluctance motor drives for EV and HEV applications,” Transportation Electrification, IEEE Transactions on, vol. 1, no. 3, pp. 245-254, 2015.

[6] F. L. M. Santos, J. Anthonis, F. Naclerio, J. J. C. Gyselinck, H. Van Der Auweraer, and L. C. S. Góes, “Multiphysics NVH Modeling : Simulation of a Switched Reluctance Motor for an Electric Vehicle,” IEEE Transaction on Industrial Electronics, vol. 61, no. 1, pp. 469-476, 2014.

[7] S. Faid, P. Debal, S. Bervoets, “Development of a switched reluctance motor for Automotive Traction Applications,” Proceedings of the 25th World Battery, Hybrid and Fuel Cell Electric Vehicle symposium & exhibition (EVS25), Shenzhen, China, pp. 5-9, 7-9 November 2010.

[8] C.T. Faria, F. Santos, F. Chauvicourt, S. Orlando, “Noise emissions on switched reluctance motors: evaluation of different structural models,” Proceedings of International Electric Vehicle Symposium and Exhibition (EVS28), Goyang, Korea, pp. 1-8, 3-6 May, 2015.

[9] L. Szabó, R. Terec, M. Ruba, P. Rafajdus, “Reconfigurable fault tolerant control system for switched reluctance motors”, Electrical and Power Engineering Frontier, 2012, vol. 1, no. 1, pp. 1-7, 2012.

[10] L. Szabó and M. Ruba “On fault tolerance increase of switched reluctance machines,” IEEE EUROCON 2009, pp. 734-739, St.-Petersburg, Russia, IEEE, 2009.

[11] P. Dubravka, P. Rafajdus, P. Makys, V. Hrabovcova and L. Szabó, “Analysis of switched reluctance motor behavior under electrical fault conditions,” Communications, 15(2 A), pp. 60-66, 2013.

[12] P. Moreno-Torres, M. Lafoz, M. Blanco, G. Navarro, J. Torres and L. García-tabarés, “Switched Reluctance Drives with Degraded Mode for Electric Vehicles,” In M. A. Fakhfakh (Ed.), Modeling and Simulation for Electric Vehicle Applications, pp. 97-124, InTech, 2016.

[13] M. Ehsani and B. Fahimi, “Elimination of position sensors in switched reluctance motor drives: state of the art and future trends,” IEEE Transactions on Industrial Electronics, vol. 49, no. 1, pp. 40-47, 2002.

[14] M. Sarrazin, J. Anthonis, H. Van der Auweraer, C.S. Marţişş, “Signature Analysis of Switched Reluctance and Permanent Magnet Electric Vehicle Drives,” Proceedings of the 2014 International Conference on Electrical Machines (ICEM 2014), IEEE, Berlin, Germany, pp. 1831–1837, 3-5 September, 2014.

[15] D. Fodorean, M. Sarrazin, C.S. Marţiş, J. Anthonis, H. Van der Auweraer, “Characterizing the motorization of a light electric vehicle through FEM and NVH tests,” Proceedings of the 2014 International Conference on Electrical Machines (ICEM 2014), IEEE, Berlin, Germany, pp. 2404–2409, 3-5 September, 2014.

[16] Y. Mollet, M. Sarrazin, H. Van der Auweraer, J. Gyselinck,“Noise and vibrations of switched reluctance machine drives - influence of the current hysteresis control,” EEA journal, vol. 64, no. 1, 2016.

[17] J. O. Fiedler, K. A. Kasper, R. W. De Doncker, “Calculation of the Acoustic Noise Spectrum of SRM Using Modal Superposition,” IEEE Trans. Ind. Electron., vol. 57, no. 9, pp. 2939-2945, 2010.

[18] J. F. Marques, J. O. Estima, N.S. Gameiro, A.J. Cardoso, “A new diagnostic technique for real-time diagnosis of power converter faults in switched reluctance motor drives,” IEEE Trans. Ind. Appl., vol. 50, no. 3, pp. 1854-1860, 2014.

[19] E. Cabal-Yepez, A.G. Garcia-Ramirez, R.J. Romero-Troncoso, A. Garcia-Perez, R.A. Osornio-Rios, “Reconfigurable monitoring system for time-frequency analysis on industrial equipment through STFT and DWT,” IEEE Trans. Ind. Inform., vol. 9, no. 2, pp. 760-771, 2013.